

Provided for non-commercial research and education use.
Not for reproduction, distribution or commercial use.



This article appeared in a journal published by Elsevier. The attached copy is furnished to the author for internal non-commercial research and education use, including for instruction at the authors institution and sharing with colleagues.

Other uses, including reproduction and distribution, or selling or licensing copies, or posting to personal, institutional or third party websites are prohibited.

In most cases authors are permitted to post their version of the article (e.g. in Word or Tex form) to their personal website or institutional repository. Authors requiring further information regarding Elsevier's archiving and manuscript policies are encouraged to visit:

<http://www.elsevier.com/copyright>



Amphiphilic multiarm star block copolymer-based multifunctional unimolecular micelles for cancer targeted drug delivery and MR imaging

Xiaojie Li^a, Yinfeng Qian^b, Tao Liu^{a,**}, Xianglong Hu^a, Guoying Zhang^a, Yezi You^a, Shiyong Liu^{a,*}

^aCAS Key Laboratory of Soft Matter Chemistry, Department of Polymer Science and Engineering, Hefei National Laboratory for Physical Sciences at the Microscale, University of Science and Technology of China, Hefei, Anhui 230026, China

^bThe First Affiliated Hospital of Anhui Medical University, Hefei, Anhui 230022, China

ARTICLE INFO

Article history:

Received 3 May 2011

Accepted 16 May 2011

Available online 12 June 2011

Keywords:

Unimolecular micelles

Targeted drug delivery

MR imaging

Multiarm star block copolymer

Theranostic nanocarriers

ABSTRACT

We report on the fabrication of multifunctional polymeric unimolecular micelles as an integrated platform for cancer targeted drug delivery and magnetic resonance imaging (MRI) contrast enhancement under in vitro and in vivo conditions. Starting from a fractionated fourth-generation hyperbranched polyester (*Boltorn H40*), the ring-opening polymerization of ϵ -caprolactone (CL) from the periphery of H40 and subsequent terminal group esterification with 2-bromoisobutyryl bromide afforded star copolymer-based atom transfer radical polymerization (ATRP) macroinitiator, *H40-PCL-Br*. Well-defined multiarm star block copolymers, *H40-PCL-b-P(OEGMA-co-AzPMA)*, were then synthesized by the ATRP of oligo(ethylene glycol) monomethyl ether methacrylate (OEGMA) and 3-azidopropyl methacrylate (AzPMA). This was followed by the click reaction of *H40-PCL-b-P(OEGMA-co-AzPMA)* with alkynyl-functionalized cancer cell-targeting moieties, *alkynyl-folate*, and T_1 -type MRI contrast agents, *alkynyl-DOTA-Gd* (DOTA is 1,4,7,10-tetraazacyclododecane-1,4,7,10-tetrakisacetic acid), affording *H40-PCL-b-P(OEGMA-Gd-FA)*. In aqueous solution, the amphiphilic multiarm star block copolymer exists as structurally stable unimolecular micelles possessing a hyperbranched polyester core, a hydrophobic PCL inner layer, and a hydrophilic P(OEGMA-Gd-FA) outer corona. *H40-PCL-b-P(OEGMA-Gd-FA)* unimolecular micelles are capable of encapsulating paclitaxel, a well-known hydrophobic anticancer drug, with a loading content of 6.67 w/w% and exhibiting controlled release of up to 80% loaded drug over a time period of ~ 120 h. In vitro MRI experiments demonstrated considerably enhanced T_1 relaxivity ($18.14 \text{ s}^{-1} \text{ mM}^{-1}$) for unimolecular micelles compared to $3.12 \text{ s}^{-1} \text{ mM}^{-1}$ for that of the small molecule counterpart, *alkynyl-DOTA-Gd*. Further experiments of in vivo MR imaging in rats revealed good accumulation of unimolecular micelles within rat liver and kidney, prominent positive contrast enhancement, and relatively long duration of blood circulation. The reported unimolecular micelles-based structurally stable nanocarriers synergistically integrated with cancer targeted drug delivery and controlled release and MR imaging functions augur well for their potential applications as theranostic systems.

© 2011 Elsevier Ltd. All rights reserved.

1. Introduction

Cancer therapy has remained to be a formidable challenge mainly due to the heterogeneity and stubborn adaptation of cancerous cells although great efforts were devoted to this field in the past several decades. Chemotherapy, as one of the most widely used tools in the long history of combating cancer diseases, still plays an important role and receives more and more scrutiny in recent years. However, traditional small molecule anticancer drugs often suffer from intrinsic limitations such as poor water solubility,

uncontrollable pharmacokinetic processes (e.g., short duration of circulation and improper biodistribution), and the possible occurrence of severe side effects, which will considerably decrease the therapeutic efficacy [1,2].

On the other hand, the physical encapsulation or covalent attachment of anticancer drug molecules into functional polymers and polymeric assemblies and other nanomaterials can offer combined advantages such as improved water solubility, higher loading capacity, sustained controlled release, prolonged in vivo circulation duration, and the specific accumulation within tumor tissues, leading to enhanced therapeutic efficacy and negligible adverse effects [3–5]. Recently, a new concept of theranostic nanomedicine, possessing integrated functions of targeted drug delivery, diagnosis, and real-time monitoring and judgment of

* Corresponding author. Tel./fax: +86 551 3607348.

** Corresponding author.

E-mail addresses: taoliu@mail.ustc.edu.cn (T. Liu), sliu@ustc.edu.cn (S. Liu).

therapeutic progresses, has been introduced to the field of cancer therapy [6,7]. It is quite promising that this type of nanocarrier design strategy might replace the traditional “one-size-fits-all” cancer therapy approach with the more personalized one, in which different patients suffering from the same type of cancer can receive tailor-made chemotherapy treatments.

As one of the most powerful *in vivo* medical diagnostic technique, magnetic resonance imaging (MRI) possesses several notable features such as high spatial and temporal resolution, no exposure to radiation, noninvasiveness, and good penetration depths and imaging sensitivity towards soft tissues [8]. Accordingly, MRI-based theranostic nanomedicine has been extensively investigated in the past few years [9,10]. A variety of MRI contrast agents (e.g., DOTA–Gd, DTPA–Gd, superparamagnetic iron oxide (SPIO) nanoparticles, and MnFe_2O_4 nanoparticles) were covalently or physically integrated with linear polymers [11,12], dendrimers [10], hyperbranched polymers [13], polymeric assemblies [14–16], proteins [17], and carbohydrates [18] to achieve synergistic functions such as drug and gene delivery, diagnosis, and imaging-guided therapy. Among them, the combination of MR imaging contrast agent with polymeric assemblies (micelles and vesicles)-based nanocarrier platform is quite appealing as the latter can endow the theranostic system with aqueous dispersibility and non-cytotoxicity for *in vivo* applications, preservation or even enhanced MR imaging performances in most cases, and improved accumulation in tumor tissues via the enhanced permeability and retention (EPR) effect.

In the pioneering work by Gao and co-workers [14], SPIO nanoparticles (MRI T_2 contrast agent) were encapsulated within hydrophobic cores of poly(ethylene oxide)-*b*-poly(ϵ -caprolactone), PEO-*b*-PCL, amphiphilic block copolymer micelles. They observed that the T_2 relaxivity (r_2) of 4 nm SPIO-loaded micelles was enhanced ~ 7 times compared to isolated hydrophilic SPIO nanoparticles due to nanoparticle clustering in the former case; moreover, the MRI detection limit was also accordingly enhanced for SPIO-loaded hybrid micelles. Later on, they further covalently modified the chain terminal of hydrophilic PEO block with cancer-targeting cRGD or lung cancer-targeting peptide (LCP); after encapsulating with SPIO nanoparticles and chemotherapeutic drug (doxorubicin, DOX) within the hydrophobic cores, the obtained drug-loaded hybrid micelles can allow for synergistic MR imaging-guided and cancer-targeted chemotherapy [19,20]. In a related work, Shuai et al. [21] reported that folate-functionalized polymeric micelles co-encapsulated with SPIO and DOX possess better targeting tropism to hepatic carcinoma cells. Manganese-doped SPIO nanoparticles were also utilized to fabricate hybrid polymeric micelles with further improved MRI contrast effects [22].

It is interesting to note that although Gd(III)-based chelating complexes is the most popular T_1 contrast agent with positive image contrast by increasing the longitudinal relaxation rates of surrounding water protons, its integration with polymeric micelles and vesicles has been far less explored. In this context, Li et al. [15] fabricated poly(L-glutamic acid)-*b*-polylactide (PGA-*b*-PLA) block copolymer micelles with the hydrophilic PGA corona covalently functionalized with DTPA–Gd complexes. The T_1 relaxivity (r_1) was enhanced ~ 2 -fold compared to small molecule contrast agent. In another two relevant reports by Yokoyama et al. [23] and Cho et al. [24], Gd³⁺-chelated micellar nanoparticles were fabricated from amphiphilic block and graft copolymers, respectively, and *in vivo* and *in vitro* MRI measurements were conducted. In both cases, considerable contrast enhancement in T_1 -weighted MR images were observed, but the detailed T_1 relaxivity values and the extent of enhancement relative to those of small molecule counterparts were not reported. Furthermore, cell-targeting moieties were not introduced in the above nanocarrier design, thus, targeted delivery of therapeutic and MRI contrast agents were not explored.

In all the above examples concerning the fabrication of new theranostic systems by integrating T_1 or T_2 contrast agents with amphiphilic block copolymer micelles, there exists an intrinsic limitation associated with the micelle structural stability. It is well-known that block copolymer micelles will disintegrate into unimers at concentrations below the critical micelle concentration (CMC). After intravenous administration, polymeric micelles will be subjected to high dilution, and other factors such as pH, temperature, ionic strength, large shear forces during blood circulation, and the presence of numerous charged blood components will also affect their structural stability [25]. This might lead to the premature release of therapeutic drugs and MRI contrast agents before they reach target tumor sites and dramatically decrease the therapeutic efficacy.

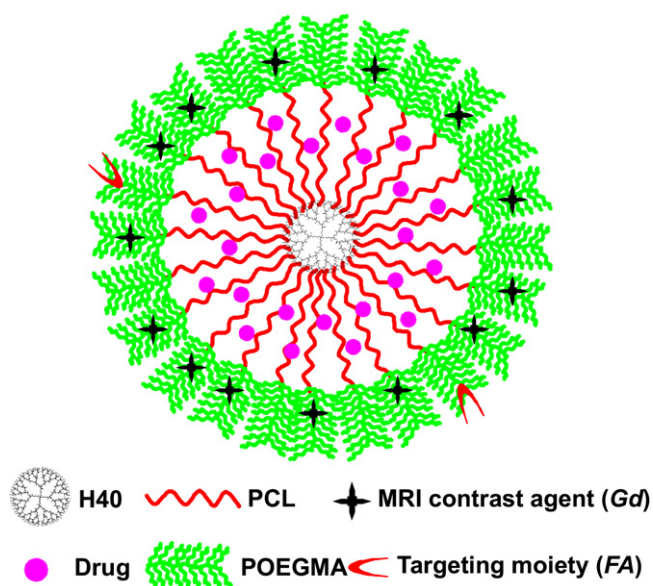
To solve the above mentioned *in vivo* structural stability issue of theranostic polymeric micelles, core and shell cross-linking approaches have been proposed. In an original example, Wooley et al. [26] covalently attached DTPA–Gd complexes onto the hydrophilic corona of shell cross-linked micelles of poly(methyl acrylate)-*b*-poly(acrylic acid) diblock copolymer (PMA-*b*-PAA). This has led to ~ 9 -fold increase in T_1 relaxivity ($r_1 = 39.0 \text{ s}^{-1} \text{ mm}^{-1}$, 0.47 T, 40 °C) as compared to small molecule DTPA–Gd complexes. Shell cross-linking endows polymeric micelles with excellent structural stability. Recently, Gong et al. [27,28] fabricated cross-linked spherical and worm-like vesicles from amphiphilic ABA triblock copolymers with the aqueous interior encapsulated with hydrophilic SPIO nanoparticles and the hydrophobic bilayers physically or covalently embedded with therapeutic drugs. In another relevant report, Jon et al. [29] coated SPIO nanoparticles with thermally cross-linked polymer inner shells and outer PEO coronas, the obtained structurally stable hybrid nanoparticles possess synergistic cancer imaging and therapeutic functions.

In addition to the above mentioned cross-linking approach to prepare stable polymeric micelles of amphiphilic block copolymers, an alternate one is to use core-shell type unimolecular micelles, which refer to nanostructured polymers with hydrophilic polymer chains covalently tethered to a hydrophobic core such as dendritic or hyperbranched polymers and multiarm star copolymers. The intrinsic covalent linkage nature between all units endows unimolecular micelles with excellent structural integrity, high loading capacity of therapeutic drugs within hydrophobic cores, and narrow disperse dimensions. Quite a few previous reports utilized polymeric unimolecular micelles as drug nanocarriers with controlled-release characteristics [30–32]. Specifically, multiarm star block copolymers were prepared from commercially available fourth-generation hyperbranched polyester (*Boltorn H40*) by employing consecutive atom transfer radical polymerizations (ATRPs) or a combination of ring-opening polymerization (ROP) and terminal coupling reactions by Klok [33], Gong [34], and Yan [35] research groups. In aqueous solution, these amphiphilic star block copolymers exist as “onion-like” three-layer unimolecular micelles possessing H40 inner cores, hydrophobic middle polymer layers, and hydrophilic outer coronas, and their applications as drug nanocarriers were also explored. We previously reported the synthesis of multiarm star and star block copolymers possessing thermo-responsive coronas by employing H40-based macroRAFT agents, and investigated the thermal phase transition behavior of unimolecular micelles in aqueous solution and their use as templates for the *in situ* generation and organization of inorganic nanoparticles [36–40].

However, amphiphilic multiarm star block copolymer-based unimolecular micelles have not been utilized to fabricate theranostic systems possessing synergistic therapeutic and MRI diagnostic functions. We expect that structurally stable core-shell type unimolecular micelles can act as excellent theranostic systems if

MRI contrast agents are integrated into the structural design and the following prerequisites are met: (1) the size of unimolecular micelles falls into the range of 20–100 nm to minimize recognition by reticuloendothelial systems; (2) the hydrophilic corona is biologically inert and generally non-cytotoxic; (3) the hydrophobic cores possess sufficient loading capacity of hydrophobic therapeutic drugs; (4) targeting moieties and T_1 contrast agents (DOTA–Gd) were covalently attached to the hydrophilic periphery to achieve cancer-targeted delivery of chemotherapeutic drugs and contrast agents.

Aiming at fulfilling the above requirements, herein we report on the fabrication of multifunctional polymeric unimolecular micelles as an integrated platform for cancer targeted drug delivery and magnetic resonance imaging (MRI) contrast enhancement under in vitro and in vivo conditions (Scheme 1). The ROP of ϵ -caprolactone (CL) from the periphery of H40 and the subsequent esterification reaction with 2-bromoisobutyryl bromide afforded star copolymer-based ATRP macroinitiator, H40-PCL-Br. Well-defined multiarm star block copolymers, H40-PCL-*b*-P(OEGMA-co-AzPMA), were then synthesized by the ATRP of oligo(ethylene glycol) monomethyl ether methacrylate (OEGMA) and 3-azidopropyl methacrylate (AzPMA). This was followed by the click reaction of H40-PCL-*b*-P(OEGMA-co-AzPMA) with alkynyl-functionalized cancer cell-targeting moieties, alkynyl-folate, and MRI contrast agents, alkynyl-DOTA–Gd (DOTA is 1,4,7,10-tetraazacyclododecane-1,4,7,10-tetrakisacetic acid), affording H40-PCL-*b*-P(OEGMA-*Gd*-FA) (Scheme 2). In aqueous solution, the amphiphilic multiarm star block copolymer exists as structurally stable unimolecular micelles possessing a hyperbranched polyester core, a hydrophobic PCL inner layer, and hydrophilic P(OEGMA-*Gd*-FA) outer corona. Subsequently, the drug encapsulation and controlled-release properties and cell-toxicity of drug-loaded H40-PCL-*b*-P(OEGMA-*Gd*-FA) unimolecular micelles were investigated and compared to non-targeted ones. In vitro and in vivo MRI contrast effects of H40-PCL-*b*-P(OEGMA-*Gd*-FA) unimolecular micelles were also explored.



Scheme 1. Schematic illustration of multifunctional unimolecular micelles based on amphiphilic multiarm star block copolymers, H40-PCL-*b*-P(OEGMA-*Gd*-FA), possessing a fourth-generation hyperbranched polyester (*Boltorn* H40) as the core, a hydrophobic poly(ϵ -caprolactone) (PCL) inner layer, and a hydrophilic outer corona of poly(oligo(ethylene glycol) monomethyl ether methacrylate) (POEGMA) covalently labeled with DOTA–Gd (*Gd*) and folic acid (FA) for synergistic targeted drug delivery and MR imaging.

2. Materials and methods

2.1. Materials

Fourth-generation hyperbranched polyester, *Boltorn* H40, from Perstorp Polyols AB was fractionated and purified following protocols reported by the Tsukruk research group [41]. GPC analysis of fractionated H40 revealed an M_n of 6500 g/mol and an M_w/M_n of 1.40. According to Tsukruk et al., the degree of branching of fractionated H40 is ~ 0.4 and the average number of monomeric units (degree of polymerization, DP) is ca. 60. ϵ -Caprolactone (CL, 99%, Acros) was dried over calcium hydride (CaH₂) and distilled prior to use. Oligo(ethylene glycol) monomethyl ether methacrylate (OEGMA, $M_n = 475$ g/mol, DP is ~ 8 –9) purchased from Aldrich was passed through a neutral alumina column to remove the inhibitor and then stored at -20 °C prior to use. 2-Bromoisobutyryl bromide (98%), copper(I) bromide (CuBr, 99%), *N,N,N',N',N''*-pentamethyldiethylenetriamine (PMDETA, 98%), stannous(II) octanoate (Sn(Oct)₂, 95%), and paclitaxel were purchased from Aldrich and used as received. Fetal bovine serum (FBS), penicillin, streptomycin, and Dulbecco's modified Eagle's medium (DMEM) were purchased from GIBCO and used as received. Tetrahydrofuran (THF) and toluene were dried by refluxing over sodium and distilled just prior to use. Triethylamine (TEA) was dried over calcium hydride (CaH₂) and distilled. All other commercially available solvents were purchased from Sinopharm Chemical Reagent Co. Ltd. and used as received. 3-Azidopropyl methacrylate (AzPMA) [42], alkynyl-functionalized folic acid, alkynyl-FA [43], and alkynyl-functionalized DOTA–Gd complex, alkynyl-DOTA–Gd (DOTA is 1,4,7,10-tetraazacyclododecane-1,4,7,10-tetrakisacetic acid) [17,44] were synthesized according to established literature procedures.

2.2. Sample synthesis

General approaches employed for the preparation of multifunctional amphiphilic hyperbranched star block copolymers, H40-PCL-*b*-P(OEGMA-*Gd*-FA), are shown in Scheme 2.

2.2.1. Synthesis of multiarm star copolymer (H40-PCL-OH) via ROP from the periphery of H40

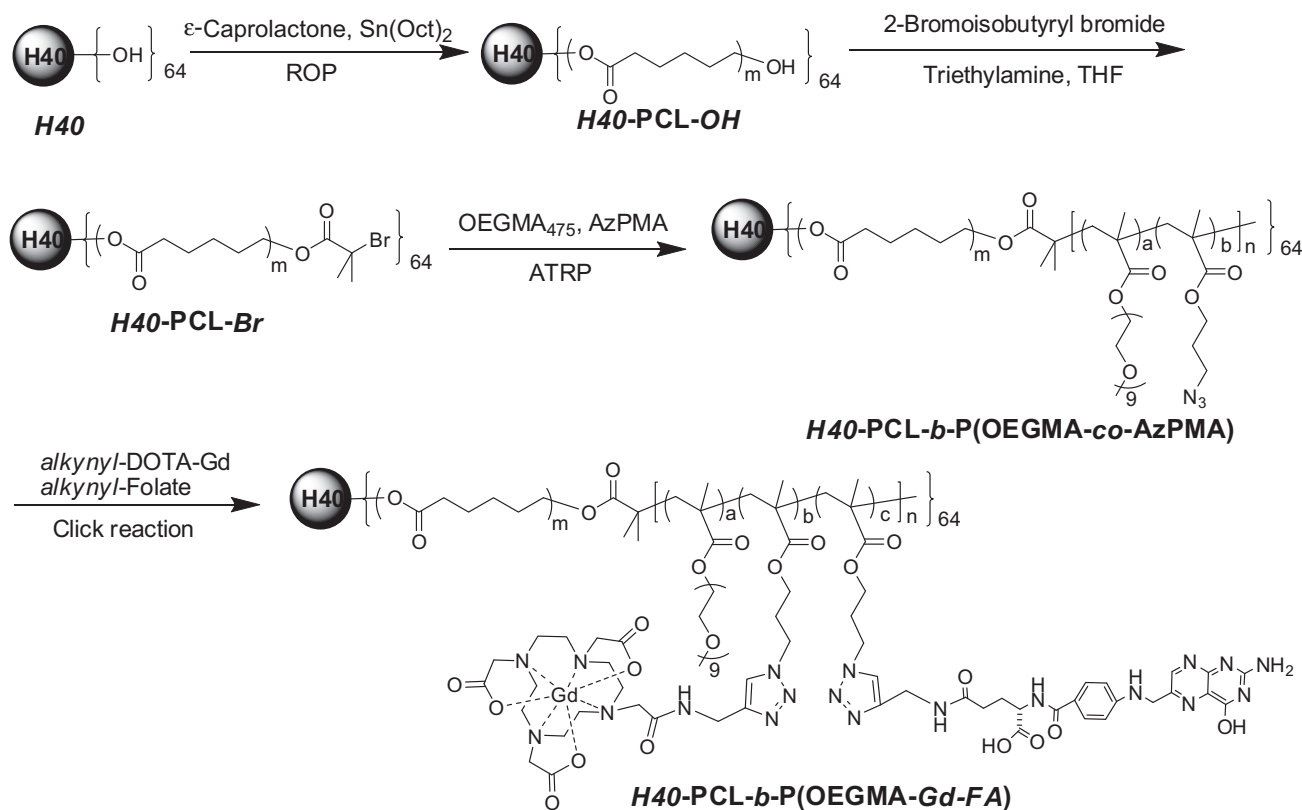
H40-(PCL)-OH was prepared by the ROP of ϵ -caprolactone using H40 as macroinitiator and Sn(Oct)₂ as the catalyst. In a typical procedure, H40 (0.30 g, 2.6 mmol hydroxyl moieties) and ϵ -caprolactone (8.9 g, 78 mmol) were charged into a 50 mL flask and heated to 130 °C under inert N₂ atmosphere. After H40 was completely dissolved in ϵ -caprolactone, a catalytic amount ([catalyst]/[hydroxyl functionalities] = 1/20) of Sn(Oct)₂ was introduced to start the polymerization. The reaction mixture was stirred for 5 h at 130 °C. After cooling to room temperature, the crude product was dissolved in THF and precipitated into an excess of the cold methanol to remove residual monomers and catalysts. The final product was dried in a vacuum oven at room temperature to afford a white powder (7.22 g, yield: 78.5%). The molecular weight and molecular weight distribution of H40-(PCL)-OH were determined by GPC using THF as the eluent, revealing an M_n of 1.52×10^5 and an M_w/M_n of 1.44 (Fig. S1a and Table 1). The DP of each PCL arm was determined to be ~ 25 based on ¹H NMR results shown in Fig. 1a.

2.2.2. Synthesis of H40-Based ATRP macroinitiator (H40-PCL-Br)

H40-PCL-OH (5.94 g, 2.0 mmol of hydroxyl functionalities) and TEA (0.41 g, 4.0 mmol) were dissolved in dry THF (50 mL) and cooled to 0 °C in an ice-water bath. 2-Bromoisobutyryl bromide (0.92 g, 4.0 mmol) in dry THF (10 mL) was added dropwise over ~ 30 min. The reaction mixture was stirred at 0 °C for another 1 h and then at room temperature for 72 h. After removal of insoluble salts by filtration, the filtrate was concentrated on a rotary evaporator and precipitated into an excess of cold methanol. The above dissolution-precipitation cycle was repeated three times. The final product was dried in a vacuum oven at room temperature to afford a white powder (5.7 g, yield: 89.1%). GPC characterization revealed an M_n of 1.82×10^5 and an M_w/M_n of 1.36 (Fig. S1b and Table 1). ¹H NMR analysis results indicated the almost quantitative transformation of terminal hydroxyl groups into ATRP initiating moieties (Fig. 1b).

2.2.3. Synthesis of H40-PCL-*b*-P(OEGMA-co-AzPMA) multiarm star block copolymers

H40-PCL-*b*-P(OEGMA-co-AzPMA) was prepared by the ATRP of OEGMA and AzPMA using H40-PCL-Br as the macroinitiator. Typically, H40-PCL-Br (0.50 g, 0.16 mmol Br moieties), OEGMA (7.6 g, 16 mmol), AzPMA (0.27 g, 1.6 mmol), PMDETA (28 mg, 0.16 mmol), and toluene (10 mL) were charged into a glass ampoule equipped with a magnetic stirring bar. The glass ampoule was degassed by three freeze-pump-thaw cycles, and then CuBr (23 mg, 0.16 mmol) and CuBr₂ (3.5 mg, 0.016 mmol) were introduced under the protection of N₂ before freezing and sealing under vacuum. After thermostating at 50 °C in an oil bath and stirring for 10 h the reaction was terminated in liquid N₂, exposed to air, and diluted with THF. The mixture was then passed through a silica gel column using THF as the eluent to remove copper catalysts. After removal of all the solvents on a rotary evaporator, the residues were dissolved in THF and precipitated into an excess of diethyl ether. The above dissolution-precipitation cycle was repeated twice. The final product was dried under vacuum overnight at room temperature (2.6 g, yield: 31.1%). GPC



Scheme 2. Synthetic routes employed for the preparation of amphiphilic multiarm star block copolymers, *H40-PCL-b-P(OEGMA-Gd-FA)*.

characterization revealed an M_n of 7.78×10^5 and an M_w/M_n of 1.23 (Fig. S1c and Table 1). Based on ^1H NMR analysis in CDCl_3 , the average DP of each P(OEGMA-co-AzPMA) block is ~ 34 and the molar content of AzPMA in P(OEGMA-co-AzPMA) block was determined to be ~ 11 mol% (Fig. 1c).

2.2.4. Synthesis of *H40-PCL-b-P(OEGMA-Gd-FA)*

H40-PCL-b-P(OEGMA-Gd-FA) was prepared by the click reaction of *H40-PCL-b-P(OEGMA-co-AzPMA)* with *alkynyl-DOTA-Gd* and *alkynyl-FA*, typical procedures employed are as follows. *H40-PCL-b-P(OEGMA-co-AzPMA)* (1.5 g, ~ 0.3 mmol azide moieties), *alkynyl-FA* (14.4 mg, 0.03 mmol), *alkynyl-DOTA-Gd* (179 mg, 0.3 mmol), PMDETA (26 mg, 0.15 mmol), and DMSO (5 mL) were added into a glass ampoule equipped with a magnetic stirring bar. The glass ampoule was degassed by three freeze-pump-thaw cycles, and then CuBr (22 mg, 0.15 mmol) was introduced under the protection of N_2 before freezing and sealing under vacuum. After thermostating at 70°C in an oil bath and stirring for 30 h the reaction was terminated in liquid N_2 , exposed to air, and diluted with THF. The mixture was then passed through a column of silica gel using THF as the eluent to remove copper catalysts. After removal of the solvents on a rotary evaporator, the residues were dissolved in THF and precipitated into an excess of diethyl ether. The product was further purified by dialysis (cellulose membrane; molecular weight cutoff, MWCO, is 3500 Da) against deionized water and lyophilized as a yellowish solid (1.54 g, yield: 92%). GPC characterization revealed an M_n of 8.1×10^5 and an M_w/M_n of 1.23 (Fig. S1d and Table 1). The number of FA molecules per multiarm star polymer was estimated to be ~ 22 by UV-vis spectroscopy in DMSO by using folic acid as the calibration standard. The Gd^{3+} content within the amphiphilic star block copolymer was determined to be

~ 2.64 wt% by inductively coupled plasma atomic emission spectrometry (ICP-AES) measurements. Thus the polymer was denoted *H40-PCL-b-P(OEGMA_{0.89}-Gd_{0.11}-FA_{0.01})₃₄* and shortened as *H40-PCL-b-P(OEGMA-Gd-FA)* in subsequent sections.

2.2.5. Fabrication of unimolecular micelles of *H40-PCL-b-P(OEGMA-Gd-FA)*

H40-PCL-b-P(OEGMA-Gd-FA) unimolecular micellar solutions at varying concentrations were prepared by a dialysis method. Briefly, *H40-PCL-b-P(OEGMA-Gd-FA)* was dissolved in 5 mL of DMF with concentrations in the range of 0.1–5.0 g/L. Then these polymer solution were directly dialyzed (cellulose membrane, molecular weight cutoff, MWCO, is 3500 Da) against deionized water for 24 h and fresh deionized water was replaced every 6 h. Final concentrations of unimolecular micellar solutions were determined by changes in total volumes inside the dialysis tube.

2.2.6. Preparation of paclitaxel-loaded unimolecular micelles

Typical procedures employed for the encapsulation of therapeutic drugs into unimolecular micelles are as follows. *H40-PCL-b-P(OEGMA-Gd-FA)* (10 mg) and paclitaxel (1 mg) were dissolved in 2.0 mL DMF. Then 8.0 mL deionized water was added dropwise into the solution under vigorous stirring over ~ 1 h. After stirring for another 2 h, the solution was dialyzed (cellulose membrane, molecular weight cutoff, MWCO, is 3500 Da) against deionized water for 24 h and fresh deionized water was replaced every 6 h. To determine the drug loading capacity, paclitaxel-loaded micellar solution was lyophilized and then dissolved in acetonitrile. The PTX loading content was calculated to be ~ 6.67 w/w% based on the UV absorption at 228 nm against a standard calibration curve.

2.3. In vitro drug release measurements

Typically, 2.5 mL paclitaxel-loaded micellar solution (1.0 g/L) of *H40-PCL-b-P(OEGMA-Gd-FA)* in phosphate buffer solution (PBS; 0.1 M, pH 7.4) was placed in a dialysis tube (cellulose membrane; molecular weight cutoff, MWCO, is 3500 Da) and then immersed into 250 mL of PBS medium under gentle stirring at 37°C . Periodically, 15 mL external buffer solution was removed and replaced with equal volume of fresh medium. Upon each sampling, the 15 mL buffer solution was lyophilized and then dissolved in acetonitrile and the paclitaxel concentration was quantified by measuring the absorbance at 228 nm against a standard curve. Each experiment was done in triple and the data are shown as the mean value plus a standard deviation (\pm SD).

Table 1

Molecular parameters of H40-based polymer precursors and amphiphilic multiarm star block copolymers used in this study.

Samples	M_n (g/mol) ^a	M_w/M_n ^a	M_n (g/mol) ^b
<i>H40-PCL-OH</i>	1.52×10^5	1.44	1.90×10^5
<i>H40-PCL-Br</i>	1.82×10^5	1.36	1.99×10^5
<i>H40-PCL-b-P(OEGMA-co-AzPMA)</i>	7.78×10^5	1.23	11.60×10^5
<i>H40-PCL-b-P(OEGMA-Gd-FA)</i>	8.10×10^5	1.23	12.98×10^5

^a Determined by GPC using THF as the eluent (1.0 mL/min).

^b Calculated from ^1H NMR results.

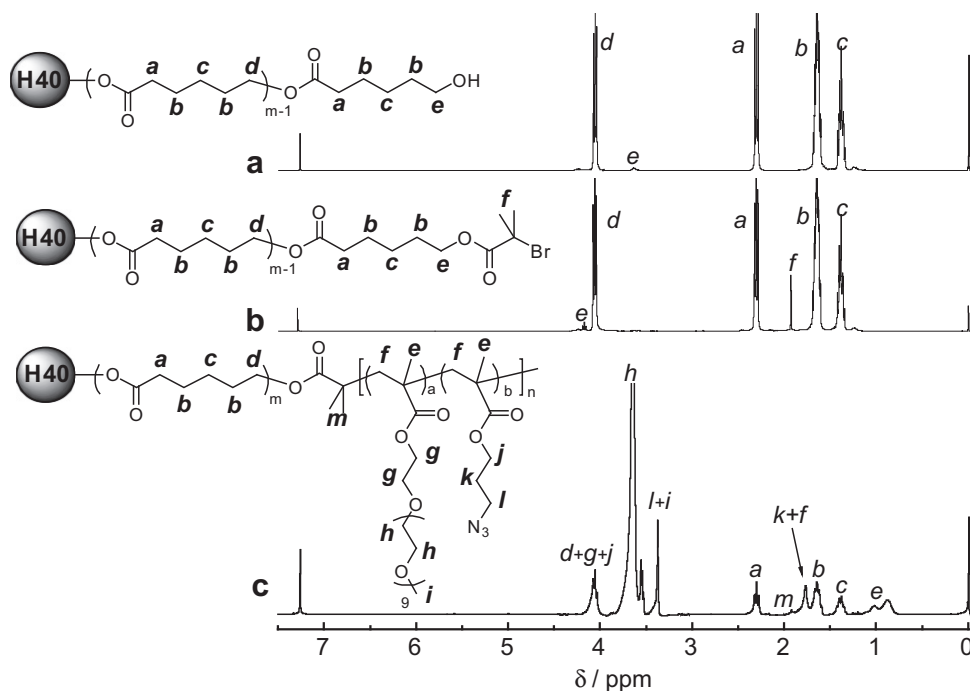


Fig. 1. ¹H NMR spectra recorded in CDCl₃ for (a) H40-PCL-OH, (b) H40-PCL-Br, and (c) H40-PCL-b-P(OEGMA-co-AzPMA).

2.4. In vitro cytotoxicity evaluation

Folate receptor overexpressing HeLa cells were employed for in vitro cytotoxicity evaluation via the MTT assay. HeLa cells were first cultured in Dulbecco's modified Eagle medium (DMEM) supplemented with 10% fetal bovine serum (FBS), penicillin (100 units/mL), and streptomycin (100 µg/mL) at 37 °C in a CO₂/air (5:95) incubator for 2 days. For cytotoxicity assay, HeLa cells were seeded in a 96-well plate at an initial density of ca. 5000 cells/well in 100 µL of complete DMEM medium. After incubating for 24 h, DMEM was replaced with fresh medium, and the cells were treated with unimolecular micellar solution at a given concentration. The treated cells were incubated in a humidified environment with 5% CO₂ at 37 °C for 48 h. The MTT reagent (in 20 µL PBS, 5 mg/mL) was added into each well. The cells were further incubated for 4 h at 37 °C. The medium in each well was then removed and replaced with 150 µL DMSO. The plate was gently agitated for 15 min before the absorbance at 570 nm was recorded by a microplate reader (Thermo Fisher). Each experiment was done in quadruple and the data are shown as the mean value plus a standard deviation (±SD).

2.5. In vitro MRI relaxivity measurement

The longitudinal relaxation rates ($1/T_1$) of H40-PCL-b-P(OEGMA-Gd-FA) unimolecular micelles and small molecule contrast agent, alkynyl-DOTA-Gd, in aqueous solution at varying Gd³⁺ concentrations (0, 0.005, 0.01, 0.02, 0.03, and 0.04 mM) were acquired at room temperature using GE Signa Horizon 1.5 T MR scanner equipped with a human shoulder coil. Conventional spin-echo pulse sequence was used for T_1 measurements with a single slice thickness of 4 mm, field of view (FOV) of 10 × 10 cm, and matrix size of 128 × 128. The repetition times (TR) were 300, 400, 500, 600, 800, 1000, 2000, and 3000 ms with an echo time (TE) of 9 ms. The net magnetizations for each sample were determined from the selected region of interest (ROI) and fit to the following multiparametric nonlinear regression function: $M_{TR} = M_0 (1 - e^{-TR/T_1})$, where M_{TR} denotes the measured signal intensity as a functional of repetition time (TR) and M_0 is the signal intensity in the thermal equilibrium [45]. T_1 were calculated from these data using a MATLAB program and longitudinal relaxivity r_1 was determined from the slope of $1/T_1$ versus [Gd³⁺] plot.

2.6. In vivo MR imaging measurement in living rats

Normal male Sprague–Dawley rats (300–350 g) were employed for in vivo investigation of small animal MR imaging. The rats were first anesthetized by intravenous injection of ketamine (80 mg/kg) and xylazine (12 mg/kg). Contrast-enhanced images of rats were obtained on a GE Signa Horizon 1.5 T MR scanner in a human shoulder coil using the Axial 3D FGRE sequence. The imaging parameters were TE = 9 ms, TR = 600 ms, 25 flip angle, 3D acquisition with 64 slices/slab,

120 mm FOV, and 0.5 mm coronal slice thickness. Each data set possesses an acquisition time of 2 min. The polymeric contrast agents were injected at a dose of 0.07 mmol Gd/kg via the tail vein into the anesthetized rat. Images were acquired at pre-injection and 2 min, 20 min, 40 min, 1 h, 20 h, and 40 h post-injection of the contrast agents. The temperature of rat was maintained between image acquisitions by using a warming pad. The effects of contrast enhancement by H40-PCL-b-P(OEGMA-Gd-FA) unimolecular micellar solution were investigated in a group of three rats. The contrast-to-noise ratio (CNR) in a specific organ was calculated using the following equation: $CNR = (S_p - S_0)/(\sigma_n)$, where S_p (post-injection) and S_0 (pre-injection) denote the signal intensity in the region of interest (ROI), and σ_n is the standard deviation of noise estimated from the background air [46].

2.7. Characterization

All nuclear magnetic resonance (NMR) spectra were recorded on a Bruker AV300 NMR 300 MHz spectrometer operated in the Fourier transform mode. CDCl₃ and DMSO-*d*₆ were used as the solvents. Two-dimensional liquid chromatography/mass spectrometry (LC/MS) was conducted on a Thermo Fisher Scientific ProteomeX-LTQ instrument. Molecular weights and molecular weight distributions were determined by gel permeation chromatography (GPC) equipped with Waters 1515 pump and Waters 2414 differential refractive index detector (set at 30 °C). It used a series of two linear Styragel columns (HR2 and HR4) at an oven temperature of 45 °C. The eluent was THF at a flow rate of 1.0 mL/min. A series of low polydispersity polystyrene standards were employed for calibration. Fourier transform infrared (FT-IR) spectra were recorded on a Bruker VECTOR-22 IR spectrometer. The spectra were collected over 64 scans with a spectral resolution of 4 cm⁻¹. Inductively coupled plasma atomic emission spectrometry (ICP-AES) (Perkin Elmer Corporation Optima 7300 DV) was used for Gd(III) content analysis. Dynamic laser light scattering (LLS) measurements were conducted on a commercial spectrometer (ALV/DLS/SL5022F) equipped with a multi-tau digital time correlator (ALV5000) and a cylindrical 22 mW UNIPHASE He–Ne laser ($\lambda_0 = 632$ nm) as the light source. Scattered light was collected at a fixed angle of 90° for duration of ~5 min. Distribution averages and particle size distributions were computed using cumulants analysis and CONTIN routines. All data were averaged over three measurements. All samples were filtered through 0.45 µm Millipore Acrodisc-12 filters to remove dust. Atomic force microscope (AFM) measurements were performed on a Digital Instrument Multimode Nanoscope IIIID operating in the tapping mode under ambient conditions. Silicon cantilever (RFESP) with resonance frequency of ~80 kHz and spring constant of ~3 N/m was used. The set-point amplitude ratio was maintained at 0.7 to minimize sample deformation induced by the tip. The sample was prepared by dip-coating unimolecular solution (0.1 g/L) onto freshly cleaved mica surface, followed by natural drying. In vitro T_1 relaxivity measurements and in vivo small animal MR imaging were recorded on a GE Signa Horizon 1.5T clinical MRI scanner.

3. Results and discussion

3.1. Synthesis and characterization of amphiphilic multiarm star block copolymers

Well-defined amphiphilic multiarm star block copolymers, *H40*-PCL-*b*-P(OEGMA-*Gd*-FA), were synthesized via the combination of ring-opening polymerization (ROP), atom transfer radical polymerization (ATRP), and click functionalization (Scheme 2). Hyperbranched star copolymer, *H40*-PCL-OH, was synthesized at first via the bulk ROP of ϵ -caprolactone (CL) using fractionated fourth-generation hyperbranched polyester (*H40*) as the macroinitiator and Sn(Oct)₂ as the catalyst at 130 °C. GPC analysis of the product revealed a relatively symmetric elution peak with an M_n of 1.52×10^5 and an M_w/M_n of 1.44 (Fig. S1a). ¹³C NMR spectra recorded for *H40* and *H40*-PCL-OH are shown in Fig. S2. Compared to those of *H40*, the complete disappearance of signals characteristic of quaternary carbons with the two adjacent hydroxyl groups remain unreacted (50.6 ppm, terminal carbon) and only one hydroxyl functionality reacted (48.4 ppm, linear carbon) in the ¹³C NMR spectrum of *H40*-PCL-OH revealed that all terminal hydroxyl groups participated in the ROP reaction. The above results agree quite well with previous relevant reports [47,48]. It is worthy of noting that the number of terminal hydroxyl groups of fractionated *H40* is very close to 64 [41]. Thus, it is reasonable to assume that *H40*-PCL-OH star copolymer possesses ~64 PCL arms. From the ¹H NMR spectrum of *H40*-PCL-OH shown in Fig. 1a, the integration ratio of peak *e* (methylene protons adjacent to the terminal hydroxyl group) to peak *a* (methylene protons adjacent to carbonyl groups) was calculated to be 1/25. Thus DP of PCL arm within *H40*-PCL-OH was determined to be ~25 by ¹H NMR.

The subsequent esterification reaction of terminal hydroxyl groups of *H40*-PCL-OH with 2-bromoisobutyryl bromide afforded *H40*-based ATRP macroinitiator, *H40*-PCL-Br, with an M_n of 1.82×10^5 and an M_w/M_n of 1.36 as revealed by GPC analysis (Fig. S1b

and Table 1). In the ¹H NMR spectrum of *H40*-PCL-Br (Fig. 1b), we can clearly observe the complete disappearance of resonance signal at 3.65 ppm characteristic of methylene protons adjacent to terminal hydroxyl groups of *H40*-PCL-OH (Fig. 1a) and the appearance of a new signal at 1.93 ppm (peak *f*, methyl protons originated from 2-bromoisobutyryl moieties). Moreover, the integral ratios of peak *f* to those characteristic of PCL repeating units further confirmed the almost quantitative transformation of the terminal hydroxyl groups into ATRP initiating functionalities (Fig. 1b).

In the next step, well-defined *H40*-PCL-*b*-P(OEGMA-*co*-AzPMA) star block copolymer was synthesized by the ATRP of OEGMA and AzPMA at 50 °C using *H40*-PCL-Br as macroinitiator. In an effort to achieve better control over the polymerization process, CuBr₂ was added as a deactivator and a relatively low monomer conversion was targeted (~30%). GPC analysis of the product revealed an M_n of 7.78×10^5 and an M_w/M_n of 1.23 (Fig. S1c). As shown in the ¹H NMR spectrum of *H40*-PCL-*b*-P(OEGMA-*co*-AzPMA) (Fig. 1c), signals characteristic resonance CL, OEGMA, and AzPMA are all present. The DP of P(OEGMA-*co*-AzPMA) block and the AzPMA content were calculated to be ~34 and ~11.0 mol%, respectively. Moreover, the presence of residual azide moieties in *H40*-PCL-*b*-P(OEGMA-*co*-AzPMA) is clearly evidenced by the characteristic absorption peak at ~2100 cm⁻¹ from the FT-IR spectrum (Fig. S3c).

Finally, multifunctional multiarm star block copolymer, *H40*-PCL-*b*-P(OEGMA-*Gd*-FA), with the hydrophilic periphery labeled with MRI contrast agent (Gd³⁺) and cancer-targeting moieties (FA) was synthesized by “click” functionalization of *H40*-PCL-*b*-P(OEGMA-*co*-AzPMA) with alkynyl-DOTA-Gd and alkynyl-FA at a [Gd]/[FA] molar ratio of 10:1 (Scheme 2). FT-IR spectrum of the final product, *H40*-PCL-*b*-P(OEGMA-*Gd*-FA), as shown in Fig. S3d qualitatively confirmed the successful click functionalization of azide moieties within *H40*-PCL-*b*-P(OEGMA-*co*-AzPMA) alkynyl-DOTA-Gd and alkynyl-FA by the disappearance of absorption peaks of ~2100 cm⁻¹ (characteristic of azide moieties) and ~2120 cm⁻¹ (characteristic of alkynyl moieties). The number of FA molecules

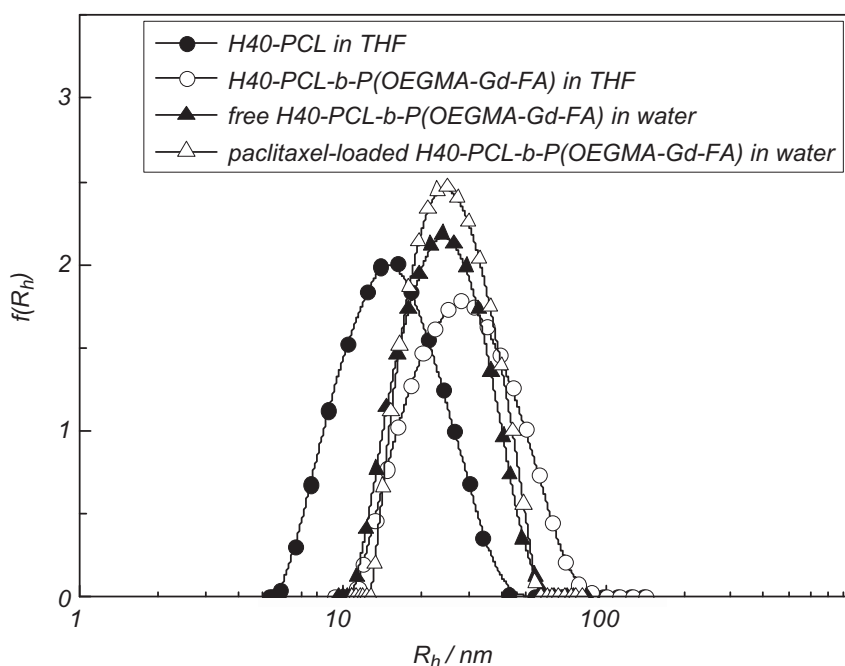


Fig. 2. Typical hydrodynamic radius distributions, $f(R_h)$, recorded for *H40*-PCL in THF solution ($\langle R_h \rangle = 15.1$ nm), *H40*-PCL-*b*-P(OEGMA-*Gd*-FA) in THF ($\langle R_h \rangle = 28.5$ nm), *H40*-PCL-*b*-P(OEGMA-*Gd*-FA) unimolecular micelles in aqueous solution ($\langle R_h \rangle = 25.2$ nm), and paclitaxel-loaded *H40*-PCL-*b*-P(OEGMA-*Gd*-FA) unimolecular micelles ($\langle R_h \rangle = 27.4$ nm). The polymer concentration is 1.0 g/L in all cases.

per multiarm star polymer was estimated to be ~ 22 by UV–vis spectroscopy in DMSO using folic acid as the calibration standard. The Gd^{3+} content within the amphiphilic star block copolymer was determined to be ~ 2.64 wt% by inductively coupled plasma atomic emission spectrometry (ICP-AES) measurements. Thus, there exist ~ 218 DOTA–Gd complexes per multiarm star block copolymer. The polymer was denoted $H40\text{-}[PCL_{25}\text{-}b\text{-}P(\text{OEGMA}_{0.89}\text{-Gd}_{0.1}\text{-FA}_{0.01})_{34}]_n$ and shortened as $H40\text{-PCL-}b\text{-}P(\text{OEGMA-Gd-FA})$ in subsequent sections.

The size and morphology of $H40\text{-PCL-}b\text{-}P(\text{OEGMA-Gd-FA})$ in THF and aqueous media were then characterized by dynamic laser light scattering (LLS) and atomic force microscopy (AFM). As shown in Fig. 2, the intensity-average hydrodynamic radius, $\langle R_h \rangle$, of $H40\text{-PCL}$ in THF was determined to be ~ 15.1 nm. By covalently attaching P(OEGMA) arms at the surface of $H40\text{-PCL}$, $\langle R_h \rangle$ of $H40\text{-PCL-}b\text{-}P(\text{OEGMA-Gd-FA})$ increased to ~ 28.5 nm. Considering that PCL arms are well-solvated under this condition due to that THF is a good solvent for PCL, $H40\text{-PCL-}b\text{-}P(\text{OEGMA-Gd-FA})$ should dissolve as unimers and exist as separate coils in THF.

In previous relevant reports concerning H40-based multiarm star block copolymers, it was observed that these amphiphilic multiarm star block copolymers might exist as unimolecular micelles or multimolecular aggregates above a critical aggregation concentration (CAC), depending on the relative block lengths of inner hydrophobic and outer hydrophilic blocks [49]. In the current study, the aqueous dispersion of $H40\text{-PCL-}b\text{-}P(\text{OEGMA-Gd-FA})$ was prepared via the cosolvent approach in combination with dialysis protocols. Dynamic LLS experiments were then conducted for the aqueous solution of $H40\text{-PCL-}b\text{-}P(\text{OEGMA-Gd-FA})$ at varying concentrations (0.1–5.0 g/L). As displayed in Fig. S4, the $\langle R_h \rangle$ of $H40\text{-PCL-}b\text{-}P(\text{OEGMA-Gd-FA})$ in aqueous solution at 1.0 g/L is determined to be ~ 25.2 nm, with is slightly lower than that in THF at the same concentration (28.5 nm, Fig. 2). This revealed that $H40\text{-PCL-}b\text{-}P(\text{OEGMA-Gd-FA})$ in aqueous solution should exist as unimolecular micelles considering the fact that the PCL inner layer remains collapsed in aqueous media. This was further confirmed by the fact that in the concentration range of 0.1–5.0 g/L, $\langle R_h \rangle$ values of $H40\text{-PCL-}b\text{-}P(\text{OEGMA-Gd-FA})$ remain almost constant (25–26 nm; Fig. S4). In addition, the scattering intensity linearly increases with polymer concentrations in the same concentration range (inset in Fig. S4), i.e., no apparent multimolecular aggregation can be observed. The above results successfully revealed that $H40\text{-PCL-}b\text{-}P(\text{OEGMA-Gd-FA})$ exist as unimolecular micelles possessing core-shell-corona type “onion-like” microstructures (Scheme 1). The morphology of $H40\text{-PCL-}b\text{-}P(\text{OEGMA-Gd-FA})$ unimolecular micelles was further investigated by AFM. As shown in Fig. 3, robust spherical nanoparticles can be clearly observed with a mean height of ~ 20 nm. The decreased dimension of the unimolecular micelles observed by AFM compared to that by dynamic LLS is reasonable considering that the former determines nanoparticle dimensions in the dry state, whereas the latter reports intensity-average dimensions in solution.

3.2. In vitro drug release and cell viability evaluation

$H40\text{-PCL-}b\text{-}P(\text{OEGMA-Gd-FA})$ unimolecular micelles possess an H40 core, an inner hydrophobic PCL layer, and a hydrophilic P(OEGMA-Gd-FA) outer corona (Scheme 1). The inner hydrophobic core was then employed to encapsulate a well-known hydrophobic anticancer drug, paclitaxel. The drug loading content and encapsulation efficiency of unimolecular micelles were determined to be ~ 6.67 wt% and $\sim 71.5\%$, respectively. After drug encapsulation, the $\langle R_h \rangle$ of unimolecular micelles slightly increased from 25.2 nm for drug-free ones to 27.4 nm for drug-loaded micelles (Fig. 2).

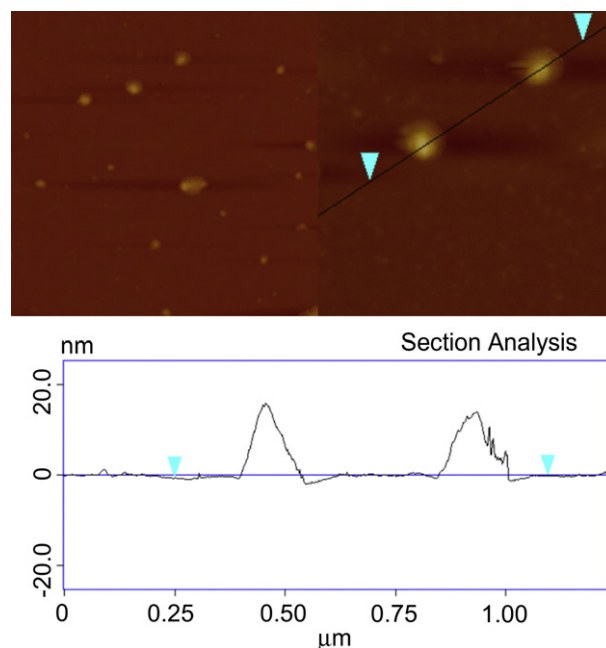


Fig. 3. AFM height images and the corresponding section analysis results recorded by drying the aqueous solution of $H40\text{-PCL-}b\text{-}P(\text{OEGMA-Gd-FA})$ (0.1 g/L) on mica.

Subsequently, in vitro drug release characteristics of paclitaxel-loaded $H40\text{-PCL-}b\text{-}P(\text{OEGMA-Gd-FA})$ unimolecular micelles was conducted under simulated physiological condition (PBS, pH 7.4, 37°C). As shown in Fig. 4, an almost linear sustained release was observed in the first 30 h with approximately 50% drug release, indicating that the unimolecular micelles are quite desirable as controlled release drug nanocarriers. At extended time periods, the release rate slowed down and reached a cumulative $\sim 80\%$ drug release after ~ 5 d.

In an effort to explore the in vitro anticancer efficacy of paclitaxel-loaded unimolecular micelles, preliminary cell viability experiments were conducted against HeLa cells. As shown in Fig. 5a, drug-free unimolecular micelles of $H40\text{-PCL-}b\text{-}P(\text{OEGMA-co-AzPMA})$ exhibit negligible cytotoxicity, i.e., $\sim 87\%$ viability at a polymer concentration up to 0.8 g/L, which is in agreement with the well-known non-cytotoxicity of PEG and PCL segments.

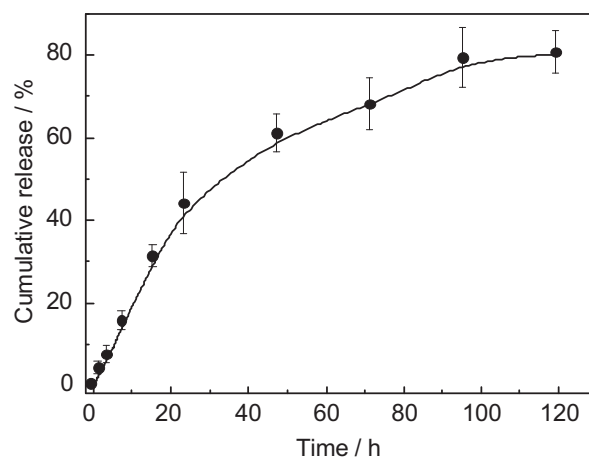


Fig. 4. In vitro release profile of paclitaxel from drug-loaded $H40\text{-PCL-}b\text{-}P(\text{OEGMA-Gd-FA})$ unimolecular micelles at 37°C (phosphate buffer; 0.1 M, pH 7.4).

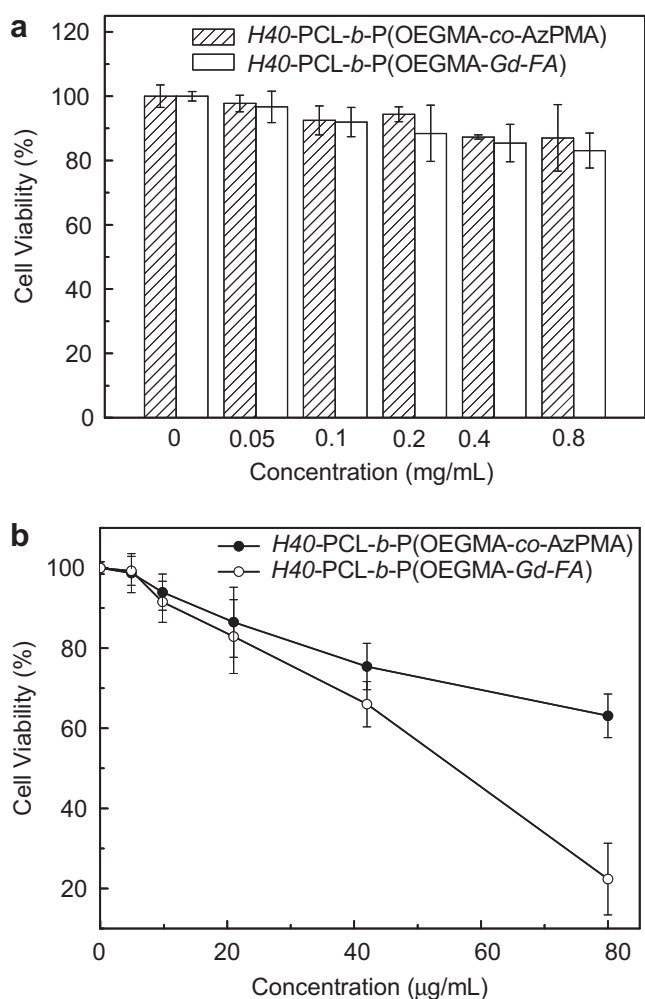


Fig. 5. (a) In vitro cytotoxicity of *H40-PCL-b-P(OEGMA-co-AzPMA)* and *H40-PCL-b-P(OEGMA-Gd-FA)* unimolecular micelles determined by MTT assay against HeLa cells. (b) Viability of HeLa cells incubated for 48 h with paclitaxel-loaded *H40-PCL-b-P(OEGMA-co-AzPMA)* and *H40-PCL-b-P(OEGMA-Gd-FA)* unimolecular micelles in aqueous solution (the drug loading content is 6.67 w/w%) at varying polymer concentrations.

Comparably, *H40-PCL-b-P(OEGMA-Gd-FA)* also exhibits negligible cytotoxicity with a cell viability of $\sim 83\%$ at a concentration of 0.8 g/L. However, by incubating HeLa cells with paclitaxel-loaded *H40-PCL-b-P(OEGMA-co-AzPMA)* unimolecular micelles, which lack of the cancer cell-targeting FA moieties, dramatically decreased cell viability was observed. At a polymer concentration of 80 $\mu\text{g/mL}$, only 63% cells remain alive (Fig. 5b). In addition, the anticancer performance can be further enhanced by introducing tumor targeting moieties, FA in this case, to the outer corona layer of unimolecular micelles. As shown in Fig. 5b, cancer cell-targeting paclitaxel-loaded *H40-PCL-b-P(OEGMA-Gd-FA)* unimolecular micelles exhibit substantially improved anticancer efficacy, with the cell viability being $\sim 23\%$ at a polymer concentration of 80 $\mu\text{g/mL}$, presumably due to the well-known folate receptor-mediated endocytosis mechanism. It is worthy of noting that in the current study, cancer-targeting FA moieties were anchored within the corona layer rather than the terminal periphery of unimolecular micelles. Considering their potential in vivo applications, the hydrophilic and inert POEGMA coronas are expected to effectively protect FA moieties from undesired enzymatic attack and premature endocytosis events during blood circulation.

3.3. In vitro MR imaging contrast enhancement of unimolecular micelles

In this section, the positive MRI contrast effects of *H40-PCL-b-P(OEGMA-Gd-FA)* unimolecular micelles were further explored. It has been well-documented that Gd^{3+} -based T_1 -type MRI contrast agents can greatly improve the diagnostic sensitivity malignant tissues from normal ones. Therefore, the combination of MRI contrast agent with polymeric assemblies-based drug delivery nanocarriers is expected to allow for the development of theranostic systems with integrated functions of MR imaging based diagnosis and cancer chemotherapy within one single ensemble. Unfortunately, small molecular Gd^{3+} -based T_1 -type MRI contrast agents often suffer from unsatisfactory sensitivity, limited circulation life within human body, and undesirable accumulation. Current research in this area focuses on the development of contrast agents with improved sensitivity, enhanced bio-distribution at targeted tumor site, and integrated with synergistic functions such as controlled or triggered release of therapeutic drugs. In the current case, *H40-PCL-b-P(OEGMA-Gd-FA)* unimolecular micelles can serve as a structurally stable nanoplatform, as compared to polymeric micelles of block copolymers, for integrated cancer-targeted MRI imaging and drug delivery.

Typical T_1 weighted spin-echo MR images recorded for *H40-PCL-b-P(OEGMA-Gd-FA)* unimolecular micelles and the small molecule counterpart, *alkynyl-DOTA-Gd*, are shown in Fig. 6a. Upon gradual increase of concentration of *alkynyl-DOTA-Gd*, we can apparently observe a positive enhancement of MR signals as revealed by the elevated brightness. Using *alkynyl-DOTA-Gd* as a reference, the corresponding *H40-PCL-b-P(OEGMA-Gd-FA)* unimolecular micellar solutions in the same Gd^{3+} concentration range

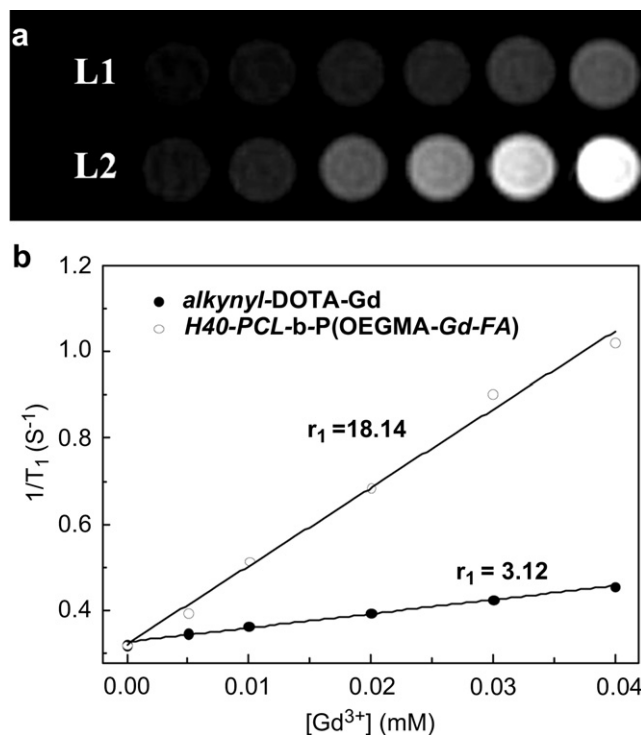


Fig. 6. (a) T_1 weighted spin-echo MR images of *alkynyl-DOTA-Gd* (L1) and *H40-PCL-b-P(OEGMA-Gd-FA)* (L2) in aqueous solution with Gd^{3+} concentrations being 0, 0.005, 0.01, 0.02, 0.03, and 0.04 mM (from left to right), respectively. Images were obtained at 1.5 T (TR/TE = 600/9 ms) at room temperature. (b) Water proton longitudinal relaxation rate ($1/T_1$) of *alkynyl-DOTA-Gd* and *H40-PCL-b-P(OEGMA-Gd-FA)* in aqueous solution as a function of Gd^{3+} concentration.

exhibits dramatically enhanced MRI signal contrast. This confirms the well-established fact that when Gd^{3+} complexes are covalently attached to polymers and polymeric assemblies, the effects of MRI contrast enhancement can be effectively improved [26].

Quantitative analysis of results shown in Fig. 6a based on Matlab software revealed an almost linear relationship between water proton longitudinal relaxation rate ($1/T_1$) and Gd^{3+} concentrations for both *alkynyl*-DOTA–Gd and *H40-PCL-b-P(OEGMA-Gd-FA)* unimolecular micelles. Small molecule *alkynyl*-DOTA–Gd possesses a T_1 relaxivity (r_1) of $3.12 \text{ s}^{-1} \text{ mM}^{-1}$, which is in general agreement with the value for commercially available DOTA–Gd complexes. However, linear regression analysis of the $1/T_1$ versus $[Gd^{3+}]$ plot for *H40-PCL-b-P(OEGMA-Gd-FA)* solution revealed a substantially increase of r_1 ($18.14 \text{ mM}^{-1} \text{ s}^{-1}$), i.e., ~ 5.8 -fold enhancement in comparison with that of *alkynyl*-DOTA–Gd. This suggests that the covalent attachment of DOTA–Gd into the hydrophilic periphery of unimolecular micelles can effectively increase the MRI contrast enhancement effects and *H40-PCL-b-P(OEGMA-Gd-FA)* can serve as excellent T_1 -type contrast agents with drug delivery nanocarrier functions.

3.4. In vivo time-dependent MRI assessment of *H40-PCL-b-P(OEGMA-Gd-FA)* unimolecular micelles

Fast clearance of small molecule therapeutic or MRI contrast agents and their poor accumulation within targeted tumor sites is a major challenge encountered for in vivo cancer chemotherapy and diagnosis. Thus, long blood circulation duration and good accumulation within targeting sites are prerequisites for the construction of high efficiency theranostic nanocarriers. Herein, PEOGMA hydrophilic shell was introduced to protect micelles in the biological milieu, thereby prolonging their blood circulation time.

After intravenous injection of *H40-PCL-b-P(OEGMA-Gd-FA)* unimolecular micelles in normal Sprague–Dawley rats, preliminary in vivo MRI contrast enhancement effects, blood circulation duration, and biodistribution of unimolecular micelles-based theranostic nanocarriers were then investigated. Fig. 7 shows MR images of a normal rat at pre-injection and at 2 min, 20 min, 40 min, 1 h, 20 h and 40 h post-injection of *H40-PCL-b-P(OEGMA-Gd-FA)* unimolecular micelles at a dose of $0.07 \text{ mmol Gd}^{3+}/\text{kg}$. A relatively strong positive MRI signal contrast enhancement throughout the whole body can be observed at $\sim 2 \text{ min}$ post-injection, indicating the fast circulation of unimolecular micelles in the bloodstream. Taking the heart as an example, we can clearly discern MRI signal enhancement at 2 min post-injection. The signal intensity then

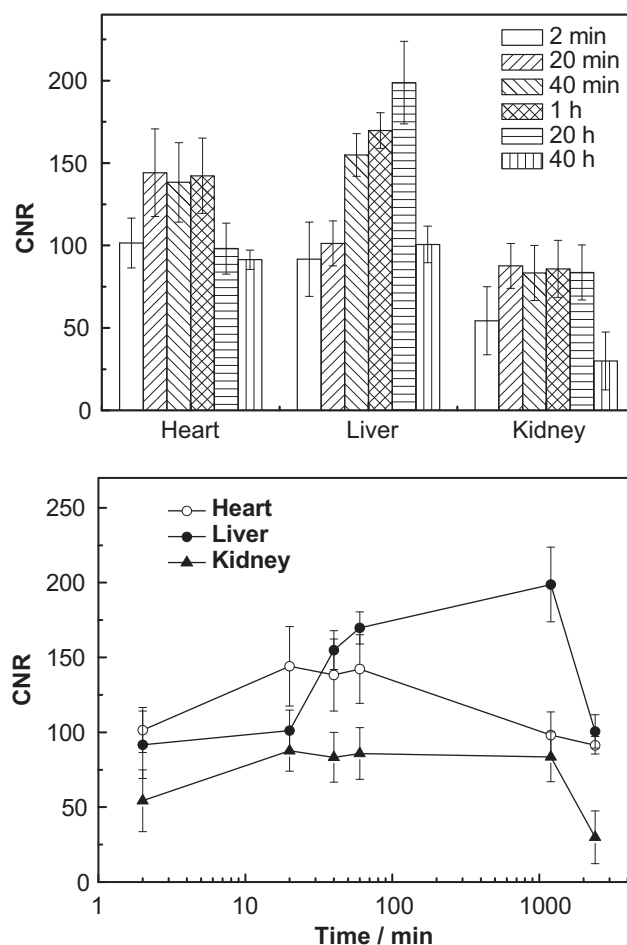


Fig. 8. Contrast-to-noise ratio (CNR) in the heart, liver and kidney of rats at pre-injection, and 2 min, 20 min, 40 min, 1 h, 20 h, and 40 h after intravenous injection of the aqueous solution of *H40-PCL-b-P(OEGMA-Gd-FA)*. The contrast agent was injected at a dose of $0.07 \text{ mmol Gd}/\text{kg}$.

reaches a maximum at 20 min post-injection and a plateau region was observed up to 1 h post-injection. Then the signal contrast enhancement considerably decreases at 20 h after injection. At 40 h post-injection, a further decrease of signal intensity can be observed within the heart organ, suggesting the decrease of the concentration of unimolecular micelles within the blood circulation. It should be noted that throughout the experimental duration,

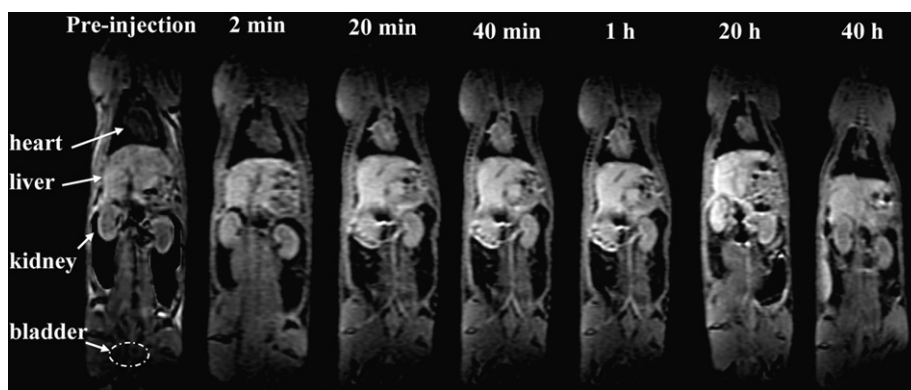


Fig. 7. MR images recorded for rats at pre-injection, and 2 min, 20 min, 40 min, 1 h, 20 h, and 40 h after intravenous injection of the aqueous solution of *H40-PCL-b-P(OEGMA-Gd-FA)* unimolecular micelles. The contrast agent was injected at a dose of $0.07 \text{ mmol Gd}/\text{kg}$.

no discernible changes of MRI signals in bladder can be observed, indicating that unimolecular micelles-based MRI contrast agents are not excreted by the glomerular filtration mechanism within kidney. This is in stark contrast with those exhibited by conventional small molecular MRI contrast agents [10].

In an effort to more accurately investigate the performance of unimolecular micelles-based MRI contrast agent, quantitative analysis was further conducted. The contrast-to-noise (CNR) ratios calculated in regions of interest (ROIs) drawn on selected organs are shown in Fig. 8. In the first 20 min, the CNR in all the major organs including heart, kidney, and liver dramatically increased, revealing the rapid circulation of unimolecular micelles within the bloodstream. Both heart and kidney reached to the highest CNR at 20 min post-injection and maintained the maximum contrast enhancement performance up to ~1 h and ~20 h, respectively. In contrast, the CNR of liver organ continuously increase in the time duration of 2 min–20 h post-injection; after reaching a maximum of signal enhancement at 20 h post-injection, the CNR starts to decrease considerably. These results indicate that *H40-PCL-b-P(OEGMA-Gd-FA)* unimolecular micelles can well accumulate within liver probably due to the presence of targeting FA moieties and the appropriate size (~50 nm in diameter) of unimolecular micelles.

4. Conclusions

In summary, amphiphilic multiarm star block copolymers, *H40-PCL-b-P(OEGMA-Gd-FA)*, were successfully synthesized as an integrated platform for cancer cell-targeted drug delivery and MR imaging contrast enhancement. In aqueous solution, the star block copolymers exist as structurally stable unimolecular micelles possessing a hydrophobic hyperbranched polyester core, a hydrophobic PCL inner layer, and a hydrophilic POEGMA outer corona covalently anchored with targeting moieties (FA) and MRI contrast agents (DOTA–Gd). The physical encapsulation of paclitaxel within the hydrophobic core of unimolecular micelles and the controlled release of them were successfully achieved. Paclitaxel-loaded cancer cell-targeting unimolecular micelles exhibit considerably higher in vitro cytotoxicity compared to non-targeting ones presumably due to the folate receptor-mediated endocytosis mechanism. In vitro MR imaging experiments revealed considerably enhanced T_1 relaxivity ($18.14 \text{ s}^{-1} \text{ mM}^{-1}$) for unimolecular micelles compared to that of small molecular DOTA–Gd complexes ($3.21 \text{ s}^{-1} \text{ mM}^{-1}$). Further in vivo MR imaging experiments in rats demonstrated prominently positive contrast enhancement and extended blood circulation duration for the reported structurally stable unimolecular micelles-based theranostic nanocarrier system.

Acknowledgments

The financial support from National Natural Scientific Foundation of China (NNSFC) Project (51033005, 20874092, 91027026, and 21090354), Fundamental Research Funds for the Central Universities, and Specialized Research Fund for the Doctoral Program of Higher Education (SRFDP) is gratefully acknowledged.

Appendix. Supplementary material

Supplementary data associated with this article can be found, in the online version, at doi:10.1016/j.biomaterials.2011.05.049.

References

[1] Sutton D, Nasongkla N, Blanco E, Gao JM. Functionalized micellar systems for cancer targeted drug delivery. *Pharm Res* 2007;24:1029–46.

- [2] Davis ME, Chen Z, Shin DM. Nanoparticle therapeutics: an emerging treatment modality for cancer. *Nat Rev Drug Discov* 2008;7:771–82.
- [3] Ferrari M. Cancer nanotechnology: opportunities and challenges. *Nat Rev Cancer* 2005;5:161–71.
- [4] Peer D, Karp JM, Hong S, Farokhzad OC, Margalit R, Langer R. Nanocarriers as an emerging platform for cancer therapy. *Nat Nanotechnol* 2007;2:751–60.
- [5] Oerlemans C, Bult W, Bos M, Storm G, Nijssen JFW, Hennink WE. Polymeric micelles in anticancer therapy: targeting, imaging and triggered release. *Pharm Res* 2010;27:2569–89.
- [6] Sumer B, Gao JM. Theranostic nanomedicine for cancer. *Nanomedicine* 2008;3:137–40.
- [7] Barreto JA, O'Malley W, Kubeil M, Graham B, Stephan H, Spiccia L. Nanomaterials: applications in cancer imaging and therapy. *Adv Mater* 2011;23:H18–40.
- [8] Mulder WJM, Strijkers GJ, van Tilborg GAF, Griffioen AW, Nicolay K. Lipid-based nanoparticles for contrast-enhanced MRI and molecular imaging. *NMR Biomed* 2006;19:142–64.
- [9] Khemtong C, Kessinger CW, Gao JM. Polymeric nanomedicine for cancer MR imaging and drug delivery. *Chem Commun*; 2009:3497–510.
- [10] Villaraza AJL, Bumb A, Brechbiel MW. Macromolecules, dendrimers, and nanomaterials in magnetic resonance imaging: the interplay between size, function, and pharmacokinetics. *Chem Rev* 2010;110:2921–59.
- [11] Vaidya A, Sun Y, Ke T, Jeong EK, Lu ZR. Contrast enhanced MRI-guided photodynamic therapy for site-specific cancer treatment. *Magn Reson Med* 2006;56:761–7.
- [12] Zarabi B, Nan AJ, Zhuo JC, Gullapalli R, Ghandehari H. HPMa copolymer-doxorubicin-gadolinium conjugates: synthesis, characterization, and in vitro evaluation. *Macromol Biosci* 2008;8:741–8.
- [13] Sideratou Z, Tsiourvas D, Theodossiou T, Fardis M, Paleos CM. Synthesis and characterization of multifunctional hyperbranched polyesters as prospective contrast agents for targeted MRI. *Bioorg Med Chem Lett* 2010;20:4177–81.
- [14] Ai H, Flask C, Weinberg B, Shuai XT, Pagel MD, Farrell D, et al. Magnetite-loaded polymeric micelles as ultrasensitive magnetic-resonance probes. *Adv Mater* 2005;17:1949–52.
- [15] Zhang GD, Zhang R, Wen XX, Li L, Li C. Micelles based on biodegradable poly(L-glutamic acid)-*b*-polylactide with paramagnetic Gd ions chelated to the shell layer as a potential nanoscale MRI-visible delivery system. *Biomacromolecules* 2008;9:36–42.
- [16] Kono K, Nakashima S, Kokuryo D, Aoki I, Shimomoto H, Aoshima S, et al. Multi-functional liposomes having temperature-triggered release and magnetic resonance imaging for tumor-specific chemotherapy. *Biomaterials* 2011;32:1387–95.
- [17] Prasuhn DE, Yeh RM, Obenaus A, Manchester M, Finn MG. Viral MRI contrast agents: coordination of Gd by native virions and attachment of Gd complexes by azide-alkyne cycloaddition. *Chem Commun*; 2007:1269–71.
- [18] Cipolla L, Gregori M, So PW. Glycans in magnetic resonance imaging: determinants of relaxivity to smart agents, and potential applications in biomedicine. *Curr Med Chem* 2011;18:1002–18.
- [19] Nasongkla N, Bey E, Ren JM, Ai H, Khemtong C, Guthi JS, et al. Multifunctional polymeric micelles as cancer-targeted, MRI-ultrasensitive drug delivery systems. *Nano Lett* 2006;6:2427–30.
- [20] Guthi JS, Yang SG, Huang G, Li SZ, Khemtong C, Kessinger CW, et al. MRI-visible micellar nanomedicine for targeted drug delivery to lung cancer cells. *Mol Pharmaceut* 2010;7:32–40.
- [21] Hong GB, Yuan RX, Liang BL, Shen J, Yang XQ, Shuai XT. Folate functionalized polymeric micelle as hepatic carcinoma-targeted, MRI-ultrasensitive delivery system of antitumor drugs. *Biomicrodevices* 2008;10:693–700.
- [22] Lu J, Ma SL, Sun JY, Xia CC, Liu C, Wang ZY, et al. Manganese ferrite nanoparticle micellar nanocomposites as MRI contrast agent for liver imaging. *Biomaterials* 2009;30:2919–28.
- [23] Shiraishi K, Kawano K, Minowa T, Maitani Y, Yokoyama M. Preparation and in vivo imaging of PEG-poly(L-lysine)-based polymeric micelle MRI contrast agents. *J Control Release* 2009;136:14–20.
- [24] Lee HY, Jee HW, Seo SM, Kwak BK, Khang G, Cho SH. Diethylene-triaminepentaacetic acid-gadolinium (DTPA–Gd)-conjugated poly-succinimide derivatives as magnetic resonance imaging contrast agents. *Bioconjug Chem* 2006;17:700–6.
- [25] Savić R, Azzam T, Eisenberg A, Maysinger D. Assessment of the integrity of poly(caprolactone)-*b*-poly(ethylene oxide) micelles under biological conditions: a fluorogenic-based approach. *Langmuir* 2006;22:3570–8.
- [26] Turner JL, Pan DPJ, Plummer R, Chen ZY, Whittaker AK, Wooley KL. Synthesis of gadolinium-labeled shell-crosslinked nanoparticles for magnetic resonance imaging applications. *Adv Funct Mater* 2005;15:1248–54.
- [27] Yang XQ, Graier JJ, Rowland IJ, Javadi A, Hurley SA, Matson VZ, et al. Multifunctional stable and pH-responsive polymer vesicles formed by heterofunctional triblock copolymer for targeted anticancer drug delivery and ultrasensitive MR imaging. *ACS Nano* 2010;4:6805–17.
- [28] Yang XQ, Graier JJ, Rowland IJ, Javadi A, Hurley SA, Steeber DA, et al. Multifunctional SPIO/DOX-loaded wormlike polymer vesicles for cancer therapy and MR imaging. *Biomaterials* 2010;31:9065–73.
- [29] Yu MK, Jeong YY, Park J, Park S, Kim JW, Min JJ, et al. Drug-loaded superparamagnetic iron oxide nanoparticles for combined cancer imaging and therapy in vivo. *Angew Chem Int Edit* 2008;47:5362–5.
- [30] Liu MJ, Kono K, Fréchet JMJ. Water-soluble dendritic unimolecular micelles: their potential as drug delivery agents. *J Control Release* 2000;65:121–31.

- [31] Zhou YF, Huang W, Liu JY, Zhu XY, Yan DY. Self-assembly of hyperbranched polymers and its biomedical applications. *Adv Mater* 2010;22:4567–90.
- [32] Schramm OG, Pavlov GM, van Erp HP, Meier MAR, Hoogenboom R, Schubert US. A versatile approach to unimolecular water-soluble carriers: ATRP of PEGMA with hydrophobic star-shaped polymeric core molecules as an alternative for PEGylation. *Macromolecules* 2009;42:1808–16.
- [33] Kreutzer G, Ternat C, Nguyen TQ, Plummer CJG, Manson JAE, Castelletto V, et al. Water-soluble, unimolecular containers based on amphiphilic multiarm star block copolymers. *Macromolecules* 2006;39:4507–16.
- [34] Prabakaran M, Grailer JJ, Pilla S, Steeber DA, Gong SQ. Amphiphilic multi-arm-block copolymer conjugated with doxorubicin via pH-sensitive hydrazone bond for tumor-targeted drug delivery. *Biomaterials* 2009;30:5757–66.
- [35] Pang Y, Liu JY, Su Y, Zhu BS, Huang W, Zhou YF, et al. Bioreducible unimolecular micelles based on amphiphilic multiarm hyperbranched copolymers for triggered drug release. *Sci China Chem* 2010;53:2497–508.
- [36] Xu J, Luo SZ, Shi WF, Liu SY. Two-stage collapse of unimolecular micelles with double thermoresponsive coronas. *Langmuir* 2006;22:989–97.
- [37] Luo SZ, Xu J, Zhu ZY, Wu C, Liu SY. Phase transition behavior of unimolecular micelles with thermoresponsive poly(*N*-isopropylacrylamide) coronas. *J Phys Chem B* 2006;110:9132–9.
- [38] Xu HX, Xu J, Zhu ZY, Liu HW, Liu SY. In-situ formation of silver nanoparticles with tunable spatial distribution at the poly(*N*-isopropylacrylamide) corona of unimolecular micelles. *Macromolecules* 2006;39:8451–5.
- [39] Xu HX, Xu J, Jiang XZ, Zhu ZY, Rao JY, Yin J, et al. Thermosensitive unimolecular micelles surface-decorated with gold nanoparticles of tunable spatial distribution. *Chem Mater* 2007;19:2489–94.
- [40] Hu JM, Liu SY. Responsive polymers for detection and sensing applications: current status and future developments. *Macromolecules* 2010;43:8315–30.
- [41] Ornatska M, Peleshanko S, Genson KL, Rybak B, Bergman KN, Tsukruk VV. Assembling of amphiphilic highly branched molecules in supramolecular nanofibers. *J Am Chem Soc* 2004;126:9675–84.
- [42] Sumerlin BS, Tsarevsky NV, Louche G, Lee RY, Matyjaszewski K. Highly efficient “click” functionalization of poly(3-azidopropyl methacrylate) prepared by ATRP. *Macromolecules* 2005;38:7540–5.
- [43] De P, Gondi SR, Sumerlin BS. Folate-conjugated thermoresponsive block copolymers: highly efficient conjugation and solution self-assembly. *Biomacromolecules* 2008;9:1064–70.
- [44] Song Y, Kohlmeier EK, Meade TJ. Synthesis of multimeric MR contrast agents for cellular imaging. *J Am Chem Soc* 2008;130:6662–3.
- [45] Bae KH, Kim YB, Lee Y, Hwang J, Park H, Park TG. Bioinspired synthesis and characterization of gadolinium-labeled magnetite nanoparticles for dual contrast T₁- and T₂-weighted magnetic resonance imaging. *Bioconjug Chem* 2010;21:505–12.
- [46] Tan MQ, Wu XM, Jeong EK, Chen QJ, Lu ZR. Peptide-targeted nanoglobular Gd–DOTA monoamide conjugates for magnetic resonance cancer molecular imaging. *Biomacromolecules* 2010;11:754–61.
- [47] Claesson H, Malmstrom E, Johansson M, Hult A. Synthesis and characterisation of star branched polyesters with dendritic cores and the effect of structural variations on zero shear rate viscosity. *Polymer* 2002;43:3511–8.
- [48] Chen S, Zhang XZ, Cheng SX, Zhuo RX, Gu ZW. Functionalized amphiphilic hyperbranched polymers for targeted drug delivery. *Biomacromolecules* 2008;9:2578–85.
- [49] Prabakaran M, Grailer JJ, Pilla S, Steeber DA, Gong SQ. Folate-conjugated amphiphilic hyperbranched block copolymers based on Boltorn (R) H40, poly(L-lactide) and poly(ethylene glycol) for tumor-targeted drug delivery. *Biomaterials* 2009;30:3009–19.